An inducible mouse model for microvillus inclusion disease reveals a role for myosin Vb in apical and basolateral trafficking

Kerstin Schneeberger[a], Georg F. Vogel[b,c], Hans Teunissen[a], Domenique D. van Ommen[d], Harry Begthel[e], Layla El Bouazzaoui[a], Anke H. M. van Vugt[a], Jeffrey M. Beekman[d], Judith Klumperman[f], Thomas Müller[g], Andreas Janecke[g,h], Patrick Gerner[i], Lukas A. Huber[b], Michael W. Hess[c], Hans Clevers[e,1], Johan H. van Es[e], Edward E. S. Nieuwenhuis[a], and Sabine Middendorp[a,1]

[a]Division of Paediatrics, Department of Paediatric Gastroenterology, Wilhelmina Children's Hospital, University Medical Centre (UMC) Utrecht, 3584 EA, Utrecht, The Netherlands; [b]Division of Cell Biology, Biocenter, Medical University Innsbruck, A-6020 Innsbruck, Austria; [c]Division of Histology and Embryology, Medical University Innsbruck, A-6020 Innsbruck Austria; [d]Laboratory of Translational Immunology and Department of Paediatric Pulmonology, Wilhelmina Children's Hospital, UMC Utrecht, 3584 EA, Utrecht, The Netherlands; [e]Hubrecht Institute for Developmental Biology and Stem Cell Research, Royal Dutch Academy of Sciences and UMC Utrecht, 3584 CT, Utrecht, The Netherlands; [f]Department of Cell Biology and The Cell Microscopy Centre, UMC Utrecht, 3584 CX, Utrecht, The Netherlands; [g]Department of Pediatrics I, Medical University Innsbruck, A-6020 Innsbruck, Austria; [h]Division of Human Genetics, Medical University Innsbruck, A-6020 Innsbruck, Austria; and [i]Zentrum für Kinder- und Jugendmedizin, Universitätsklinikum Freiburg, 79106 Freiburg, Germany

Contributed by Hans Clevers, August 28, 2015 (sent for review March 30, 2015)

Microvillus inclusion disease (MVID) is a rare intestinal enteropathy with an onset within a few days to months after birth, resulting in persistent watery diarrhea. Mutations in the myosin Vb gene (*MYO5B*) have been identified in the majority of MVID patients. However, the exact pathophysiology of MVID still remains unclear. To address the specific role of MYO5B in the intestine, we generated an intestine-specific conditional *Myo5b*-deficient (*Myo5b$^{fl/fl}$;Vil-CreERT2*) mouse model. We analyzed intestinal tissues and cultured organoids of *Myo5b$^{fl/fl}$;Vil-CreERT2* mice by electron microscopy, immunofluorescence, and immunohistochemistry. Our data showed that *Myo5b$^{fl/fl}$;Vil-CreERT2* mice developed severe diarrhea within 4 d after tamoxifen induction. Periodic Acid Schiff and alkaline phosphatase staining revealed subapical accumulation of intracellular vesicles in villus enterocytes. Analysis by electron microscopy confirmed an almost complete absence of apical microvilli, the appearance of microvillus inclusions, and enlarged intercellular spaces in induced *Myo5b$^{fl/fl}$;Vil-CreERT2* intestines. In addition, we determined that MYO5B is involved not only in apical but also basolateral trafficking of proteins. The analysis of the intestine during the early onset of the disease revealed that subapical accumulation of secretory granules precedes occurrence of microvillus inclusions, indicating involvement of MYO5B in early differentiation of epithelial cells. By comparing our data with a novel MVID patient, we conclude that our mouse model completely recapitulates the intestinal phenotype of human MVID. This includes severe diarrhea, loss of microvilli, occurrence of microvillus inclusions, and subapical secretory granules. Thus, loss of MYO5B disturbs both apical and basolateral trafficking of proteins and causes MVID in mice.

mouse model | myosin Vb | epithelila polarity | intestinal enteropathy | microvillus inclusion disease

Microvillus inclusion disease (MVID) is a rare intestinal enteropathy with autosomal recessive inheritance, which was first described in 1978 (1). MVID patients cannot take up any nutrients and are often completely dependent on parenteral nutrition. The disease is characterized by villus atrophy, (partial) loss of microvilli on the apical plasma membrane of intestinal epithelial cells, and accumulation of intracellular vesicles/vacuoles, containing apical proteins and microvilli (2, 3). In addition, some studies also show mislocalization of apical and basolateral proteins, occasional crypt hyperplasia, and villus fusion (4–6).

In the great majority of patients, MVID is caused by mutations in *MYO5B*, encoding the motorprotein, myosin Vb (5). In two patients, mutations in syntaxin 3 (*STX3*) caused a variant form of MVID (7). More than 41 unique mutations along the different regions in *MYO5B* have been identified in MVID patients, including deletions and nonsense, missense, and splice-site mutations (8–10). *MYO5B* is coding for the actin-based myosin 5b motor protein, which regulates apical membrane trafficking (5, 11). MYO5B functions as a homodimer and has three functional domains: an N-terminal motor domain, a calmodulin-binding domain, and a C-terminal tail, which binds cargo through association with the small GTPases RAB8A and/or RAB11A (12, 13). Altered expression of myosin Vb affects the apical membrane trafficking mechanism in epithelial cells, causing mislocalization of apical brush border proteins, such as villin (*vil*), CD10, or alkaline phosphatase (ALP) in the cytoplasm of duodenal enterocytes (2, 3, 5), and an increased apical localization of transferrin receptor (5, 14).

Although mouse models mimicking certain features of MVID have previously been described, such as *Rab8* (15), *Cdc42* (16, 17), and *Rab11a* knockout (KO) mice (18, 19), no mutations in the coding regions of those genes have been reported in human MVID patients. Current in vitro models to study apical trafficking and polarization-associated diseases such as MVID are the parental Caco2 cell line, Caco-BBE, and LS174 W4 cells, in which polarization can be induced in vitro (4, 8, 12, 20). Although valuable knowledge about the function of MYO5B in polarization

Significance

Microvillus inclusion disease (MVID) is a rare intestinal enteropathy resulting in severe diarrhoea in neonates. Here, we have generated an intestine-specific knockout mouse model for Myosin Vb, the gene causing MVID in the majority of human patients. Our mouse model completely recapitulates the intestinal human MVID phenotype, including severe diarrhoea, loss of microvilli, occurrence of microvillus inclusions, and subapical secretory granules in villus enterocytes. In addition, we identify a newly identified role of Myo5b in trafficking of basolateral proteins, in the apical localization of the brush border membrane fusion protein syntaxin 3 (STX3), and in early differentiation of enterocytes. Our data indicate a role of MYO5B in regulating polarity of epithelial cells and have important implications for future treatment options for MVID patients.

Author contributions: K.S., H.C., J.H.v.E., E.E.S.N., and S.M. designed research; K.S., G.F.V., H.T., D.D.v.O., H.B., L.E.B., A.H.M.v.V., A.J., and M.W.H. performed research; J.M.B., J.K., T.M., P.G., L.A.H., and M.W.H. contributed new reagents/analytic tools; K.S., G.F.V., D.D.v.O., M.W.H., and S.M. analyzed data; and K.S. and S.M. wrote the paper.

The authors declare no conflict of interest.

[1]To whom correspondence may be addressed. Email: h.clevers@hubrecht.eu or s.middendorp@umcutrecht.nl.

This article contains supporting information online at www.pnas.org/lookup/suppl/doi:10.1073/pnas.1516672112/-/DCSupplemental.

was gained in these models, the direct relevance of the colon cancer cell lines for the disease is questionable, and diverging results have been obtained with knockdown of *MYO5B* in the parental Caco2 cells compared with the more polarized Caco-BBE cells (8, 12, 20). As such, we here present an inducible MVID mouse model that recapitulates the genetic defects in man, which allows analysis of the role of MYO5B in a physiological setting and the sequence of events in MVID pathophysiology.

Results

Generation of Mice. To study the consequence of *Myo5b* ablation in an in vivo model, we generated a Cre-inducible floxed *Myo5b* mouse in which *LoxP* sites were placed around exon 4 (Fig. 1*A*). Targeted ES cell clones were checked for homologous recombination by Southern blotting (Fig. S1*A*). Cre-induced deletion of exon 4 in our mouse model results in a frame shift and a premature stop codon leading to a truncated protein of 111 amino acids (a full-length protein is 1,818 amino acids) and loss of the MYO5B protein. To generate an intestine-specific inducible KO mouse model for *Myo5b*, we have crossed homozygous *Myo5b*$^{fl/fl}$ mice with a *Vil-CreERT2* mouse strain (21). *Vil-CreERT2* mice express the Cre enzyme under the control of the *Vil* promoter, which drives stable and homogeneous expression of the Cre recombinase in all epithelial cells of the small and large intestine. Because the Cre recombinase is fused to the estrogen receptor ERT2, it remains retained in the plasma membrane of

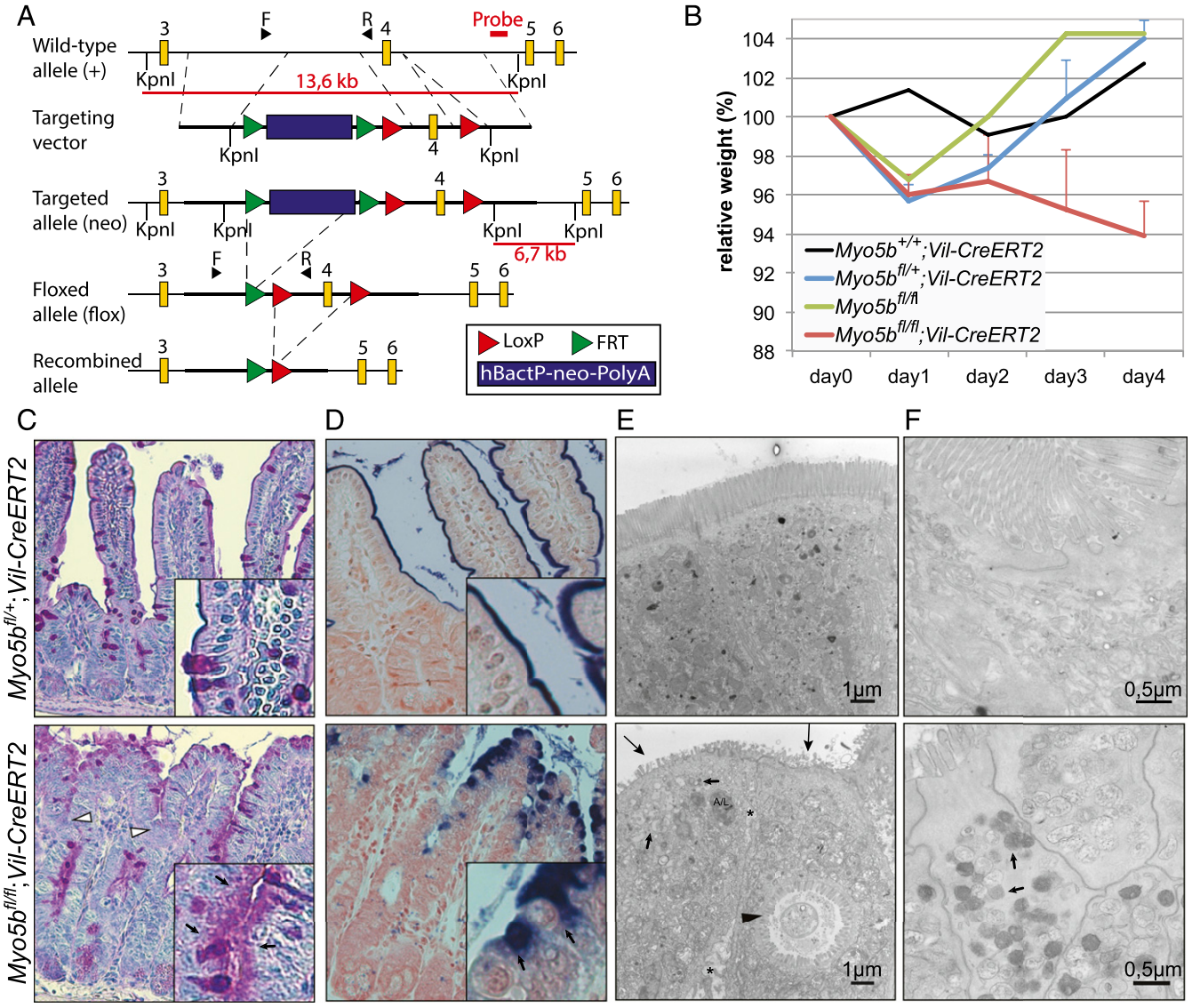

Fig. 1. Myo5b deficiency causes an MVID phenotype in mice. (*A*) Diagram depicting the strategy for the conditional KO of exon 4 of the *Myo5b* gene. The probe used for Southern blot analysis (indicated in red) hybridizes with a 13.6-kb KpnI fragment from the wild-type allele and with a 6.7-kb KpnI fragment from the targeted allele. F and R indicate the location of the primers used for genotyping. Exons are indicated with yellow squares. *LoxP* sites and *FRT* sites are represented by red and green triangles, respectively. (*B*) Relative weight curves of homozygous *Myo5b*$^{fl/fl}$*;Vil-CreERT2* mice (n = 2–8 per time point), heterozygous *Myo5b*$^{fl/+}$*;Vil-CreERT2* control mice (n = 2–6 per time point), one *Myo5b*$^{+/+}$*;Vil-CreERT2*, and one *Myo5b*$^{+/+}$ control mouse. All mice were induced with 4.5 mg tamoxifen at 8–10 wk of age. Graph shows means + SEM. (*C*–*E*) At day 4 after induction, *Myo5b*$^{fl/fl}$*;Vil-CreERT2* mice showed (*C*) subapical accumulation of PAS-positive vesicles (small arrows) and villus fusion (white arrowheads) and (*D*) mislocalization of the apical marker ALP to the cytoplasm (arrows). (*E* and *F*) TEM revealed (*E*) erosion and loss of apical microvilli (large arrows), subapical accumulation of vesicles (small arrows), intracellular microvillus inclusions (black arrowhead), A/Ls, and widened intercellular spaces (*) in villus epithelial cells of *Myo5b*$^{fl/fl}$*;Vil-CreERT2* mice. (*F*) EM-cytochemistry shows epithelial cells at the crypt–villus transition with PAS-positive, classical secretory granules (small arrows).

Table 1. Quantification of TEM characteristics

MVID characteristics	*Myo5b*$^{fl/+}$;*Vil-Cre* (n = 50)	*Myo5b*$^{fl/fl}$;*Vil-Cre* (n = 100)	P value
Microvillus inclusions	0%	19%	0.0004
Apical microvilli	100%	20%	<0.0001
Basolateral microvilli	0%	20%	0.0002
A/Ls	30%	78%	<0.0001
Subapical accumulation of vesicles	4%	73%	<0.0001
Increased intercellular space	6%	50%	<0.0001

Five *Myo5b*$^{fl/fl}$;*Vil-Cre* and two *Myo5b*$^{fl/+}$;*Vil-Cre* mice were injected with tamoxifen and killed 4 d later. TEM was performed, and 50–100 enterocytes per mouse strain were analyzed for MVID characteristics.

the epithelial cells. Only upon induction with tamoxifen, the CreERT2 protein is translocated to the nucleus, where it can promote recombination of the *LoxP* sites and thereby inactivate the conditional *Myo5b* allele. The resulting *Myo5b*$^{fl/fl}$;*Vil-CreERT2* mice were genotyped by PCR (Fig. S1*B*).

To determine the intestine-specific phenotype of loss of *Myo5b*, we have injected *Myo5b*$^{fl/fl}$;*Vil-CreERT2* mice and *Myo5b*$^{+/+}$;*Vil-CreERT2*, *Myo5b*$^{fl/+}$;*Vil-CreERT2*, and *Myo5b*$^{fl/fl}$ control mice with tamoxifen and measured their weight every day. Starting from day 3 after tamoxifen induction, only *Myo5b*$^{fl/fl}$;*Vil-CreERT2* mice displayed severe weight loss compared with controls (Fig. 1*B*). Mice were killed no later than day 4 after induction, due to severe weight loss and dehydration as a result from watery diarrhea (Fig. S1*C*). We observed that *Myo5b*$^{+/+}$;*Vil-CreERT2*, *Myo5b*$^{fl/+}$;*Vil-CreERT2*, and *Myo5b*$^{fl/fl}$;*Vil-CreERT2* control mice did not show any phenotype, as confirmed by weight curves, Periodic Acid Schiff (PAS) staining and EM (Fig. 1*B* and Fig. S1*D*). Absence of myosin Vb upon tamoxifen induction was confirmed by mRNA expression and immunohistochemistry (Fig. S2 *A* and *B*).

Loss of Myo5b Causes MVID Phenotype in Mice. The histological analysis of the intestine of the tamoxifen-induced *Myo5b*$^{fl/fl}$;*Vil-CreERT2* mice on day 4 showed villus atrophy and crypt hyperplasia, which was confirmed by a significantly ($P < 0.0001$) increased amount of Ki67-positive crypt cells (Fig. 1 *C* and *D* and Fig. S2 *C* and *D*). We have counted 23 ± 0.4 and 29 ± 0.6 Ki67^{+} cells in 50 crypts from a *Myo5b*$^{fl/+}$;*Vil-CreERT2* and a *Myo5b*$^{fl/fl}$;*Vil-CreERT2* mouse, respectively (Fig. S2*D*). Furthermore, PAS and ALP staining revealed subapical accumulation of intracellular vesicles in villus enterocytes. Finally, fusion of villi was observed, a feature only recently reported from MVID patients (4) (Fig. 1 *C* and *D*).

Pathognomonic features of MVID are the so-called microvillus inclusions that are found in ∼10% of mature enterocytes at the tips of the villi of these patients (3, 22). Analysis of the intestines of induced *Myo5b*$^{fl/fl}$;*Vil-CreERT2* mice by electron microscopy (EM) showed a severe reduction to almost complete absence of apical microvilli on day 4 after induction. Furthermore, we found conspicuous clusters of subapical vesicles as well as (auto)lysosomes (A/Ls) and microvillus inclusions in mature villus enterocytes (Fig. 1*E*). Finally, we observed enlarged intercellular spaces between enterocytes and occasionally basolateral microvilli. Strongly PAS-positive vesicles, representing the classical electron-dense secretory granules (3), occurred in crypt enterocytes and at the crypt–villus transition (Fig. 1*F*). The features described above have been reported to be the main pathological features of MVID patients (1, 3, 5, 8, 11, 14), indicating that our mouse model phenocopies human MVID. Additionally, we have quantified the phenotypic characteristics of our mouse model in Table 1.

STX3 and RAB11A Define Microvillus Inclusions as Apical Domains. Previously, it has been shown that MYO5B regulates localization of apical proteins toward the plasma membrane (2, 4, 5, 8, 9, 14, 20, 23, 24). In concordance with previous findings, ALP staining showed subapical accumulation in villus enterocytes of *Myo5b*$^{fl/fl}$;*Vil-CreERT2* mice (Fig. 1*D*). Furthermore, phosphorylated Ezrin–Radixin–Moesin (pERM), which connects the apical plasma membrane to F-actin filaments to stabilize microvilli (25–27), was markedly decreased at the apical membrane and was found in the cytoplasm of *Myo5b*$^{fl/fl}$;*Vil-CreERT2* mice (Fig. 2 *A* and *B*).

To perform its function, MYO5B associates with RAB8A and RAB11A, working as a tether and connecting Rab-associated vesicles to actin filaments (9, 12). Depending on the association with either RAB8A or RAB11A, MYO5B is involved in distinct trafficking pathways. MYO5B association with RAB8A has been linked to direct trafficking from the Golgi to the plasma membrane, whereas association of MYO5B with RAB11A is crucial for apical endosomal recycling (13).

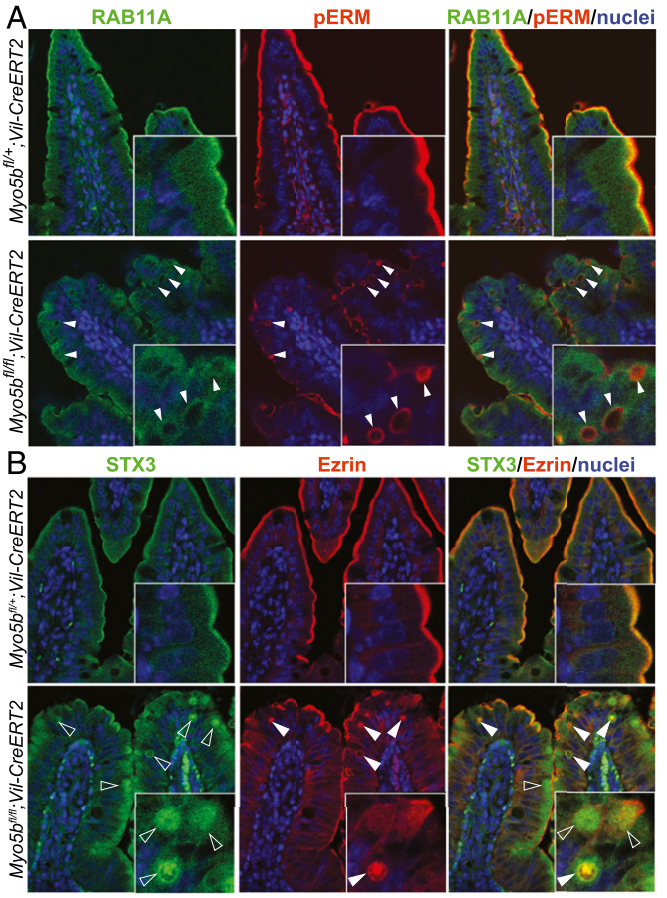

Fig. 2. Apical proteins mislocalize to inclusions that are surrounded by RAB11A. Coimmunofluorescence staining for (*A*) pERM with RAB11A and (*B*) ezrin with STX3 on day 4 after Cre induction revealed a loss of apical pERM (arrows) and occurrence of pERM/ezrin-positive microvillus inclusions (closed arrowheads) in *Myo5b*$^{fl/fl}$;*Vil-CreERT2* mice, which costained with STX3 (open arrowheads) and are surrounded by RAB11A.

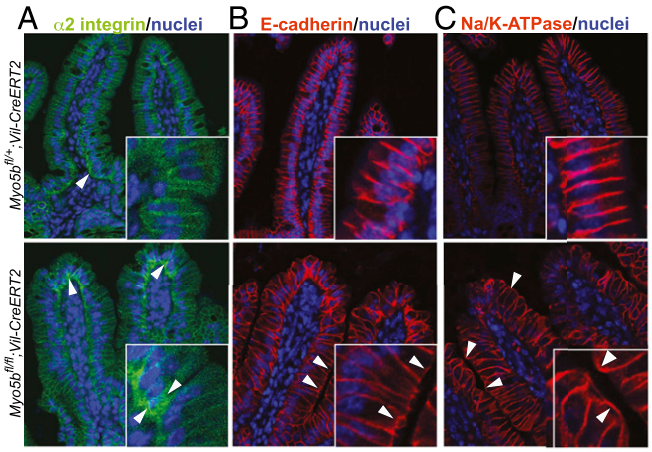

Fig. 3. Basolateral proteins are mislocalized. On day 4 after induction with tamoxifen, *Myo5b*$^{fl/fl}$*;Vil-CreERT2* intestines displayed mislocalization of the basolateral markers (*A*) α2 integrin to the basolateral cytoplasm of enterocytes at the tip of the villus (arrowheads) and (*B*) E-cadherin and (*C*) Na/K-ATPase to the apical membrane (arrowheads).

Here, we show that control mice show diffuse staining of RAB8A and subapical staining of RAB11A. In contrast, *Myo5b*$^{fl/fl}$*; Vil-CreERT2* mice show reduced RAB8A staining with a few subapical foci (Fig. S3*A*). RAB11A was lost at the apical membrane and showed a more diffuse cytoplasmic staining. In addition, several intracellular ezrin-positive inclusions were surrounded by RAB11A-positive vesicles (Fig. 2*A*). Lysosome-associated membrane protein 1 (LAMP1), which normally localizes subapically, was diffusely distributed in the cytoplasm of *Myo5b*$^{fl/fl}$*;Vil-CreERT2* enterocytes (Fig. S3*B*). These data indicate a disturbed trafficking and recycling machinery in *Myo5b*-deficient cells.

Previously, we have shown that, next to MYO5B, the target-soluble *N*-ethylmaleimide–sensitive factor attachment protein receptor (t-SNARE) protein STX3 is also involved in MVID pathogenesis, as we described two patients with a variant form of MVID having mutations in *STX3* (7). Furthermore, in a *Rab11*-KO mouse model, it was reported that microvillus inclusions were associated with STX3 (18). Here, we show that the ezrin-positive inclusions in our *Myo5b*-KO mouse model colocalize with STX3 (Fig. 2*B*). This indicates that microvillus inclusions present as ectopic apical domains positive for the apical t-SNARE STX3 and being surrounded by RAB11A-positive vesicles.

Loss of Myo5b Causes Disturbed Basolateral Polarity. Data on basolateral markers in different MVID patients or *MYO5B*-deficient cell lines are not consistent, and basolateral polarity seems not always to be disturbed (2, 5, 12, 14). We analyzed the localization of selected basolateral markers and found that 4 days after tamoxifen induction, *Myo5b*$^{fl/fl}$*;Vil-CreERT2* mice showed a slightly abnormal distribution of α2-integrin. This integrin subunit is mainly expressed on basolateral membranes of lower villus enterocytes. Notably, in *Myo5b*$^{fl/fl}$*;Vil-CreERT2* mice, enterocytes at the tip of the villus showed stronger staining at the basal plasma membrane and near the nucleus (Fig. 3*A*). E-cadherin and Na/K-ATPase, which are normally only located at the basolateral membrane, were found on apical surfaces of some, but not all, Myo5b-deficient cells (Fig. 3 *B* and *C*).

***Myo5b*$^{fl/fl}$*;Vil-CreERT2* Mice Phenocopy Human MVID.** As summarized in Table 1, all histological characteristics found in MVID patients were phenocopied in our *Myo5b*$^{fl/fl}$*;Vil-CreERT2* mouse model. To better compare mouse and human disease phenotypes, we additionally show the analysis of a newly identified MVID patient, harboring a homozygous c.1323–2A > G splice-site mutation in *MYO5B*, identified previously in MVID (5). EM shows loss of microvilli, subapical accumulation of vesicles/secretory granules, basolateral microvilli, and microvillus inclusions (Fig. 4*A*). EM-cytochemistry for PAS-reactive material revealed strongly positive vesicles at the crypt–villus transition of the MVID patient, which represents classical ("dark") secretory granules (Fig. 4*B*). Furthermore, costainings on cryosections show that intracellular actin-positive inclusions are surrounded by RAB11A (Fig. 4*C*) and the basolateral Na/K-ATPase was partly mislocalized to the apical membrane (Fig. 4*D*). Actin-positive inclusions colocalized with STX3 (Fig. 4*E*), and LAMP1 was distributed more diffusely throughout the cytoplasm of MVID enterocytes (Fig. 4*E*).

In conclusion, the analysis of the MVID patient fully confirms the validity of the mouse model presented here presented (see Table S1 for a summary).

Loss of Myo5b First Affects Immature Enterocytes and Consecutively Leads to Disturbed Recycling in Mature Enterocytes. In MVID patients, the most severe phenotype is observed in mature villus enterocytes at the tip of the villi, whereas crypt cells appear less

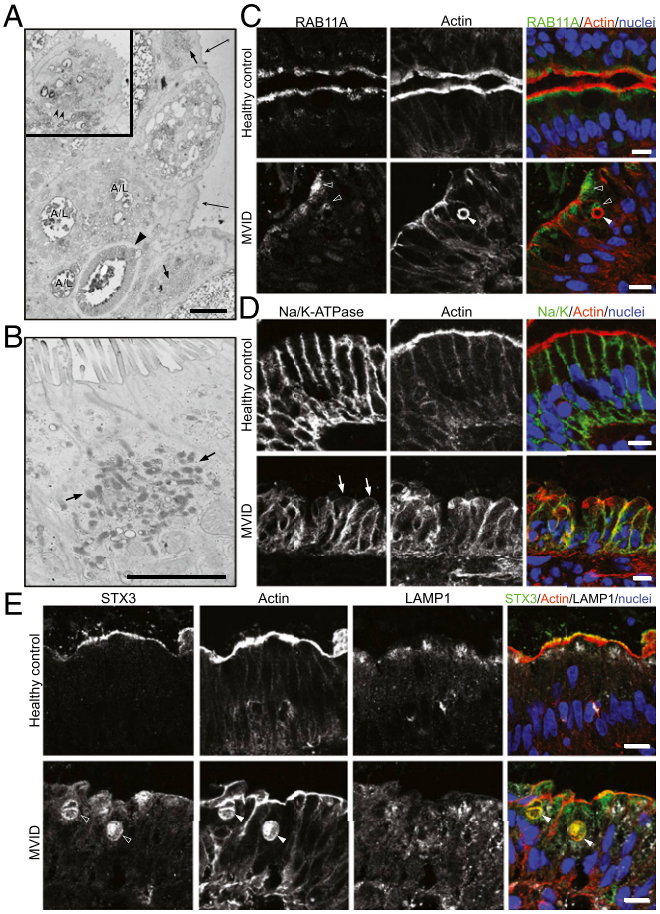

Fig. 4. Phenotypic analysis of a newly identified human MVID patient with a MYO5B 1323–2A > G mutation. (*A*) TEM shows loss of microvilli (big arrows), subapical accumulation of translucent vesicles (small arrows), A/Ls, and microvillus inclusions (arrowhead). The *Inset* shows basolateral microvilli (double arrowhead). (*B*) EM-cytochemistry for PAS-positive material shows classical electron-dense, secretory granules (arrows) in epithelial cells at the crypt–villus transition. (*C–E*) Costainings on crysections show that actin-positive inclusions (arrowheads) are (*C*) surrounded by RAB11A-positive vesicles (open arrowheads) and (*D*) colocalizing with STX3. (*E*) LAMP1 is localized more diffusely in the cytoplasm and does not colocalize with actin inclusions in the MVID patient. [Scale bar, (*A* and *B*) 2 μm and (*C–E*) 10 μm.]

CELL BIOLOGY

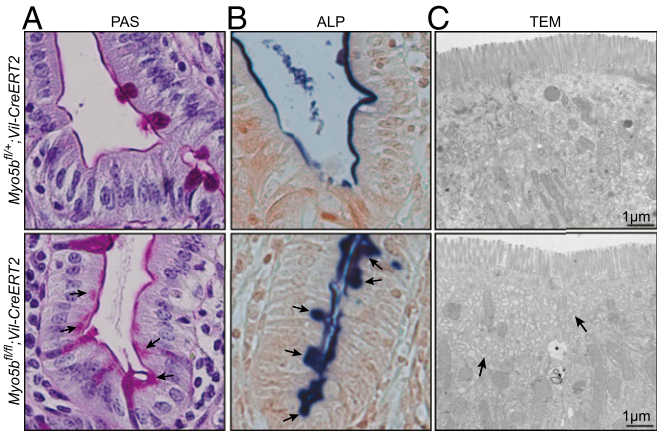

Fig. 5. Lower villus cells are the first cells affected by loss of MYO5B. *Myo5b*$^{fl/+}$*;Vil-CreERT2* and *Myo5b*$^{fl/fl}$*;Vil-CreERT2* mice were killed 2 d after tamoxifen injection. (*A*) PAS and (*B*) ALP staining located subapically in epithelial cells at the crypt–villus transition and lower villus (arrows). (*C*) TEM confirmed subapical accumulation of vesicles (arrows) and widened intercellular space (*) in lower villus cells of *Myo5b*$^{fl/fl}$*;Vil-CreERT2* mice.

affected (5, 14). In our mouse model, we analyzed the effects of loss of Myo5b in immature and mature epithelial cells over time. On day 1 after induction, we still observed MYO5B protein by immunohistochemistry in the intestines, and as such we did not observe any phenotype.

We confirmed the loss of Myo5b from day 2 after induction onwards. On day 2, cells in the upper part of the villus displayed a normal morphology, whereas the more immature cells at the crypt–villus transition and lower villus cells showed intracellular accumulation of PAS-positive material (Fig. 5*A*), cytoplasmic ALP staining (Fig. 5*B*), and accumulation of subapical vesicles (Fig. 5*C*). However, at this time point, we did not observe pERM-positive microvillus inclusions. In contrast, at day 4 after induction, all enterocytes along the villi were affected.

Collectively, these data show that loss of Myo5b first affects differentiation at the crypt–villus transition, leading to subapical accumulation of secretory granules. Consecutively, *Myo5b* deficiency disturbs apico-basolateral polarity, reflected by the occurrence of pERM/Ezrin/STX3-positive microvillus inclusions and defective RAB11A-dependent recycling.

***Myo5b*$^{fl/fl}$*;Vil-CreERT2* Organoids Represent an in Vitro Model for MVID and Reveal Impaired Functionality of Intestinal Epithelial Cells.** To perform detailed cellular and functional analysis of *Myo5b*-deficient intestinal epithelial cells, we established intestinal organoids from *Myo5b*$^{fl/fl}$*;Vil-CreERT2* mice (28). Noninduced organoids from *Myo5b*$^{fl/fl}$*;Vil-CreERT2* mice showed the same morphology as wild-type control organoids (Fig. 6*A*). Upon in vitro activation of Cre recombinase with 4-hydroxytamoxifen (4-OHT) for 15 h, the organoids appeared more compact with less budding structures and more cell death (Fig. 6*A*). By histology and TEM, we confirmed that the induced organoids reflect MVID, including intracellular accumulation of apical proteins such as ALP (Fig. 6*B*), microvillus inclusions, and absence of microvilli (Fig. 6*C*).

We applied this in vitro model for MVID to assess the functional capacities of *Myo5b*-deficient intestinal epithelial cells. It was previously shown that apical localization of the Cystic Fibrosis Transmembrane Conductance Regulator (CFTR) in polarized epithelial cells is MYO5B-dependent (2, 24). As such, we have performed Forskolin-Induced Swelling (FIS) assays, which measure the functional activity of the CFTR anion channel (29). Upon stimulation with forskolin, cAMP/protein kinase A-mediated phosphorylation of CFTR, for instance, enables opening of various ion channels, thereby facilitating transport of anions and fluids into the lumen of the organoids, which leads to swelling. Here we show that within 24 h upon Cre induction, *Myo5b*-deficient organoids are less able to swell upon stimulation with forskolin compared with control organoids (Fig. 6*D*). These data indicate that loss of Myo5b affects functional capacities of intestinal epithelial cells and myosin Vb is involved in the forskolin-dependent activation of CFTR and perhaps other basolateral ion channels or transporters required for the cAMP-induced secretory response.

Discussion

In this study, we describe an intestine-specific conditional *Myo5b* KO mouse model, in which loss of *Myo5b* can be induced by tamoxifen injection. We showed that our model completely recapitulates the disease phenotype of human MVID patients carrying *MYO5B* mutations (Table S1).

Patients usually present with severe diarrhea within the first days after birth (3). Similarily, *Myo5b*-deficient mice developed watery diarrhea within 4 days after induction (Fig. 1*B* and Fig. S1*C*). We demonstrated that loss of *Myo5b* led to an almost complete absence of enterocyte brush border, accumulation of intracellular vesicles, and occurrence microvillus inclusions (Fig. 1 *C*–*E*). Myo5b is known to interact with RAB8A or RAB11A (13). Both GTPases are involved in epithelial polarity. Furthermore, *Rab8a* and *Rab11a* KO mice displayed MVID-like phenotypes (15, 18, 19). However, the phenotypes observed in these mouse models were less severe

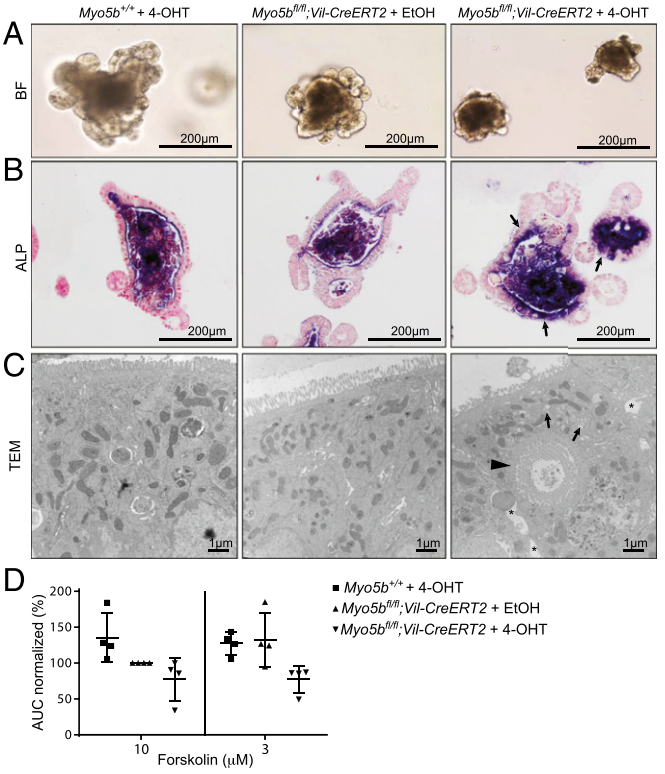

Fig. 6. Myo5b-deficient organoids represent an in vitro model for MVID. *Myo5b*$^{fl/fl}$ and *Myo5b*$^{fl/fl}$*;Vil-CreERT2* organoids were treated in vitro with 1 μM 4-OHT or vehicle control (EtOH) for 15 h and analyzed 3 d later for (*A*) morphology by brightfield (BF) microscopy, (*B*) ALP staining showing subapical accumulations (arrows), and (*C*) TEM showing subapical accumulation of vesicles (small arrows), intracellular microvillus inclusions (arrowhead), and intercellular space (*) in 4-OHT–treated *Myo5b*$^{fl/fl}$*;Vil-CreERT2* organoids. (*D*) FIS assays were performed 24 h after in vitro treatment with 4-OHT or EtOH. CFTR-mediated swelling of the organoids was measured after 40 min of incubation with 10 or 3 μM forskolin. Swelling was calculated relative to the area under the curve (AUC) of *Myo5b*$^{fl/fl}$*;Vil-CreERT2* organoids that were treated with EtOH and 10 μM forskolin. Graph shows means ± SD of quadruplicate measurements of four independent experiments.

than in our *Myo5b*-deficient mice, with a shortening but no absence of apical microvilli, and mice dying only within 2 wk (*Rab11* KO) or 5 wk (Rab8 KO) after birth (15, 18, 19).

This suggests that Myo5b acts in different trafficking pathways, dependent on its association with either RAB8A or RAB11A, and that the severe phenotype observed in patients and in our mouse model results from the combined disturbance of both pathways.

In our inducible mouse model, we observed dispersal of both RAB8A and RAB11A. Similar RAB11A staining patterns were observed in the MVID patient. Interestingly, in *Myo5b*$^{fl/fl}$*;Vil-CreERT2* mice, only RAB11A but not RAB8A accumulated around pERM/Ezrin-positive microvillus inclusions (Figs. 2 and 4 and Fig. S3). This is in concordance with previous findings that only the loss of MYO5B binding to RAB11A caused the formation of microvillus inclusions in Caco-BBE cells (12). Because normal apical recycling through the apical recycling endosome is RAB-dependent, we suggest that this process is disturbed in MVID. Furthermore, we conclude that microvillus inclusions are an ectopic apical domain within the cytoplasm of enterocytes, as they contain the apical t-SNARE STX3 and are surrounded by RAB11A-positive vesicles, which are usually found subapically.

Recently, it was suggested that stabilization of initial cell polarity might be a future target for therapy of MVID patients (12, 17). Here, we confirmed that a normal pERM-containing brush border was present at an early time point (day 2) after induction, and microvillus inclusions were mainly formed in mature enterocytes at a late time point (day 4). However, despite formation of brush border, apical polarity was already affected in the immature enterocytes at the crypt–villus junction on day 2 after induction, represented by subapical accumulation of ALP- and PAS-positive vesicles (Fig. 5). Moreover, using organoids from *Myo5b*$^{fl/fl}$*;Vil-CreERT2* mice, we show that already on day 1 after induction, the functionality of the epithelial cells was impaired, as they showed reduced swelling upon stimulation with forskolin (Fig. 6). Importantly, at that time point after splitting, the organoids do not contain mature enterocytes yet (28), confirming again that immature enterocytes are also affected in polarity and function upon loss of MYO5B. Stabilization of early brush border formation might therefore not be effective, and a stem cell-based therapy might be necessary as a future treatment for MVID patients.

Materials and Methods

A detailed description of materials and methods can be found in the *SI Materials and Methods*.

Generation of Mice. We generated a conditional *Myo5b* allele by inserting two *LoxP* sites around exon 4. Male chimaeras were subsequently crossed to C57BL/6 females, and germ-line transmission was confirmed by PCR. The neomycin expression cassette was excised in vivo by crossing the mice with *Flp1* transgenic mice (29). For intestinal epithelium-specific KO, *Myo5b*$^{fl/fl}$ mice were crossed to a *Vil-CreERT2* line. All animal procedures were performed in accordance with local animal welfare laws and guidelines and were reviewed by the Animal Ethics Committee of the Royal Dutch Academy of Sciences.

Human Material. We studied biopsies from a 4-wk-old female Turkish patient. The study was approved by the Ethics committee of the Medical University of Innsbruck (study no. UN3987), and written informed consent from the parents was obtained.

(Immuno)histochemistry and Immunofluorescence. Stainings were performed as described previously (17). An overview of all antibodies used, their dilutions, incubation times, and antigen retrieval can be found in Table S2.

Transmission Electron Microscopy. Transmission electron microscopy (TEM) was performed as described previously (30).

Organoid Culture. Small intestinal organoids were established from WT and *Myo5b*$^{fl/fl}$*;Vil-CreERT2* mice as described previously (26).

Note Added in Proof. During the review and revision process, the following paper was published, reporting another Myo5b mouse model for MVID (31).

ACKNOWLEDGMENTS. We thank Jeroen Korving for blastocyst injections and George Posthuma, Cecilia de Heus, Karin Gutleben, Barbara Witting, Caroline Hermann, and animal caretakers for (technical) assistance. This work is supported by Netherlands Organisation for Scientific Reserach (NWO) VIDI 016.146.353 (to S.M.) and NWO Translational Adult Stem Cell Research 40-41400-98-1108 (to H.C. and E.E.S.N.) and by the Molecular Cell Biology and Oncology PhD program of the Austrian Research Funds (to L.A.H.).

1. Davidson GP, Cutz E, Hamilton JR, Gall DG (1978) Familial enteropathy: A syndrome of protracted diarrhea from birth, failure to thrive, and hypoplastic villus atrophy. *Gastroenterology* 75(5):783–790.
2. Ameen NA, Salas PJ (2000) Microvillus inclusion disease: A genetic defect affecting apical membrane protein traffic in intestinal epithelium. *Traffic* 1(1):76–83.
3. Cutz E, et al. (1989) Microvillus inclusion disease: An inherited defect of brush-border assembly and differentiation. *N Engl J Med* 320(10):646–651.
4. Dhekne HS, et al. (2014) Myosin Vb and Rab11a regulate phosphorylation of ezrin in enterocytes. *J Cell Sci* 127(Pt 5):1007–1017.
5. Müller T, et al. (2008) MYO5B mutations cause microvillus inclusion disease and disrupt epithelial cell polarity. *Nat Genet* 40(10):1163–1165.
6. Thoeni CE, et al. (2014) Microvillus inclusion disease: Loss of Myosin vb disrupts intracellular traffic and cell polarity. *Traffic* 15(1):22–42.
7. Wiegerinck CL, et al. (2014) Loss of syntaxin 3 causes variant microvillus inclusion disease. *Gastroenterology* 147(1):65–68.e10.
8. Ruemmele FM, et al. (2010) Loss-of-function of MYO5B is the main cause of microvillus inclusion disease: 15 novel mutations and a CaCo-2 RNAi cell model. *Hum Mutat* 31(5):544–551.
9. Szperl AM, et al. (2011) Functional characterization of mutations in the myosin Vb gene associated with microvillus inclusion disease. *J Pediatr Gastroenterol Nutr* 52(3):307–313.
10. van der Velde KJ, et al. (2013) An overview and online registry of microvillus inclusion disease patients and their MYO5B mutations. *Hum Mutat* 34(12):1597–1605.
11. Erickson RP, Larson-Thomé K, Valenzuela RK, Whitaker SE, Shub MD (2008) Navajo microvillous inclusion disease is due to a mutation in MYO5B. *Am J Med Genet A* 146A(24):3117–3119.
12. Knowles BC, et al. (2014) Myosin Vb uncoupling from RAB8A and RAB11A elicits microvillus inclusion disease. *J Clin Invest* 124(7):2947–2962.
13. Roland JT, et al. (2011) Rab GTPase-Myo5B complexes control membrane recycling and epithelial polarization. *Proc Natl Acad Sci USA* 108(7):2789–2794.
14. Sato T, et al. (2007) The Rab8 GTPase regulates apical protein localization in intestinal cells. *Nature* 448(7151):366–369.
15. Melendez J, et al. (2013) Cdc42 coordinates proliferation, polarity, migration, and differentiation of small intestinal epithelial cells in mice. *Gastroenterology* 145(4):808–819.
16. Sakamori R, et al. (2012) Cdc42 and Rab8a are critical for intestinal stem cell division, survival, and differentiation in mice. *J Clin Invest* 122(3):1052–1065.
17. Knowles BC, et al. (2015) Rab11a regulates syntaxin 3 localization and microvillus assembly in enterocytes. *J Cell Sci* 128(8):1617–1626.
18. Sobajima T, et al. (2014) Rab11a is required for apical protein localisation in the intestine. *Biol Open* 4(1):86–94.
19. Kravtsov D, et al. (2014) Myosin 5b loss of function leads to defects in polarized signalling: Implication for Microvillus Inclusion Disease pathogenesis and treatment. *Am J Physiol Gastrointest Liver Physiol* 307(10):G992–G1001.
20. el Marjou F, et al. (2004) Tissue-specific and inducible Cre-mediated recombination in the gut epithelium. *Genesis* 39(3):186–193.
21. Reinshagen K, Naim HY, Zimmer KP (2002) Autophagocytosis of the apical membrane in microvillus inclusion disease. *Gut* 51(4):514–521.
22. Hales CM, Vaerman JP, Goldenring JR (2002) Rab11 family interacting protein 2 associates with Myosin Vb and regulates plasma membrane recycling. *J Biol Chem* 277(52):50415–50421.
23. Swiatecka-Urban A, et al. (2007) Myosin Vb is required for trafficking of the cystic fibrosis transmembrane conductance regulator in Rab11a-specific apical recycling endosomes in polarized human airway epithelial cells. *J Biol Chem* 282(32):23725–23736.
24. Garbett D, LaLonde DP, Bretscher A (2010) The scaffolding protein EBP50 regulates microvillar assembly in a phosphorylation-dependent manner. *J Cell Biol* 191(2):397–413.
25. Morales FC, Takahashi Y, Kreimann EL, Georgescu MM (2004) Ezrin-radixin-moesin (ERM)-binding phosphoprotein 50 organizes ERM proteins at the apical membrane of polarized epithelia. *Proc Natl Acad Sci USA* 101(51):17705–17710.
26. Saotome I, Curto M, McClatchey AI (2004) Ezrin is essential for epithelial organization and villus morphogenesis in the developing intestine. *Dev Cell* 6(6):855–864.
27. Dukes JD, et al. (2011) Functional ESCRT machinery is required for constitutive recycling of claudin-1 and maintenance of polarity in vertebrate epithelial cells. *Mol Biol Cell* 22(17):3192–3205.
28. Sato T, et al. (2009) Single Lgr5 stem cells build crypt-villus structures in vitro without a mesenchymal niche. *Nature* 459(7244):262–265.
29. Dekkers JF, et al. (2013) A functional CFTR assay using primary cystic fibrosis intestinal organoids. *Nat Med* 19(7):939–945.
30. Raymond CS, Soriano P (2007) High-efficiency FLP and PhiC31 site-specific recombination in mammalian cells. *PLoS One* 2(1):e162.
31. Cartón-Garcia F, et al. (2015) Myo5b knockout mice as a model of microvillus inclusion disease. *Sci Rep* 5:12312.
32. Middendorp S, et al. (2014) Adult stem cells in the small intestine are intrinsically programmed with their location-specific function. *Stem Cells* 32(5):1083–1091.